Manufacturing Rev. **8**, 9 (2021)

https://doi.org/10.1051/mfreview/2021006

Manufacturing Review
Available online at:
https://mfr.edp-open.org

RESEARCH ARTICLE OPEN ACCESS

Influence of aluminium content on the microstructure and densification of spark plasma sintered nickel aluminium bronze

Avwerosuoghene Moses Okoro*, Senzeni Sipho Lephuthing, Samuel Ranti Oke, and Peter Apata Olubambi

Centre for Nanomechanics and Tribocorrosion, Department of Metallurgy, School of Mining, Metallurgy and Chemical Engineering, University of Johannesburg, Republic of South Africa

Received: 21 December 2020 / Accepted: 14 February 2021

Abstract. In this study, nickel aluminium bronze alloys (NAB) with appreciable densification and improved microhardness was consolidated via spark plasma sintering technique. The NAB alloy was synthesized from starting elemental powders comprised nickel (4 wt.%), aluminium (6, 8 & 10 wt.%) and copper using dry milling technique. Starting powders were homogeneously milled using gentle ball mill for 8 h at a speed of 150 rpm and a BPR of 10:1. Subsequently, the milled powders were consolidated using the spark plasma sintering technique at 750 °C under a compressive pressure of 50 MPa and rate of heating (100 °C/min). Furthermore, the powders and sintered alloys were characterized using SEM and XRD to ascertain the microstructural and phase evolutions during the synthesis of the NAB. The density and microhardness of the alloys were further investigated to ascertain the integrity of the sintered alloys. The results indicated that the increase in aluminium content resulted in the formation of intermetallic and beta phases on the alloy after sintering and the microhardness of the alloys improved with the increase in aluminium content.

Keywords: Spark plasma sintering / nickel aluminium bronze / microstructure / densification / hardness

1 Introduction

Nickel aluminium bronze alloys (NAB) are extensively desirable for oil and gas as well as marine applications especially for the production of pumps, impellers, pipes owing to its outstanding strength and degradation resistance in turbulence corrosive environments [1,2]. The NAB alloys have complex composition and microstructures that requires appropriate manufacturing technique and heat treatment to unveil its unique properties [3]. Basically, this alloy usually contains aluminium (6–13 wt.%), nickel (Ni) up to 7 wt.% and copper (Cu). In some cases, iron can be added up to 7 wt.% to the alloy to refine the grain structures and improve the tensile strength, while manganese up to 1.5 wt.% is added as a deoxidizing agent and strengthening elements [3,4]. The presence of aluminium (Al) in the alloy promotes the strength and corrosion resistance while nickel stabilizes the microstructures, increase the strength and corrosion resistance.

The complex as-cast NAB microstructure is usually made up of coarse grains with Widmanstätten alpha (α) phases, trapped beta (β) phases and kappa (κ) phases which is usually formed as precipitates resulting from the presence of the various alloying elements [5]. The conventional casting techniques used in the fabrication of NAB results in the formation of segregated coarse grains with micropores, which significantly affects the mechanical properties of the alloy [6,7]. In addition, the formation of (κ) precipitates in the as-cast alloy adversely affect the corrosion resistance, mechanical properties and wear behaviours of the alloy [8,9]. Therefore, the formation of micropores alongside the segregated coarse grain structures in as-cast NAB have limited their widespread applications in structural engineering components.

In recent times, the synthesis of advanced materials using the powder metallurgy (PM) route has proven effective especially during the production of materials with complex microstructures [10,11]. The PM route has advantages over conventional casting techniques for producing materials with uniform microstructures and less segregated grains, which result in improved material properties. Spark plasma sintering (SPS) is an innovative manufacturing and efficient method used for fabricating materials with complex microstructures. The SPS technique has been extensively employed to fabricate various

* e-mail: okoromo@gmail.com

material systems namely composites, alloys, ceramics and polymers [12]. This technique uses pulse direct current alongside compressive pressure to rapidly consolidate materials without allowing significant grain growth. In addition, the SPS technique is highly desirable over other conventional fabrication technique, because it can be utilized to consolidate materials to achieve higher densification within a short period at a lower temperature.

In a bid to synthesis NAB alloy with improved densification and microhardness, the SPS technique was employed in this study to fabricate NAB with varying concentration of aluminium and the influence of aluminium content on the density and microhardness was investigated.

2 Materials and method

Nickel aluminium bronze powders were produced from the individual elemental powder components (Cu, Ni and Al). The Cu powders used has spherical particles with average sizes of ~85.7 µm. Similarly, the Ni and Al powders comprise spherical particles with average sizes of ~29.5 and ~15.4 µm respectively. In order to form a homogenous NAB powder, the elemental powders were dry milled in a gentle ball mill (Retch PM 100) for 8 h at a speed of 150 revolutions per minute using a BPR of 10:1. Alumina balls of 5 mm diameter were utilized as the milling media to achieve the uniformity of the milled powders. The milled powders were produced with aluminium (6, 8 and 10 wt.%), nickel (4 wt.%) and copper. Thereafter, the influence of the various aluminium content in the NAB alloy was evaluated to ascertain the best alloy grade.

Table 1. Shows the elemental constituent of the fabricated NAB alloy.

NAB	Aluminium (wt.%)	Nickel (wt.%)	Copper (wt.%)
NAB1	6	4	90
NAB2	8	4	88
NAB3	10	4	86

Subsequently, the milled powders were cold compacted to achieve green strength in a Ø20 mm diameter graphite die at a load of 10 KN and then fabricated using the SPS (model HHPD-25, FCT GmbH Germany) technique. The 10 KN load was used to cold compact the mixed and starting powders to achieve green strength and aid good conductivity between the powders and the graphite die before it is transferred to the SPS sintering chamber. The fabricated samples have a thickness of 5 mm and it was fabricated using the following sintering parameters; 50 MPa, 5 min, 100 °C/min and 750 °C. The composition of the NAB alloys is presented in Table 1.

Thereafter, the sintered NAB alloys were sandblasted to remove impurities and the relative densities were measured in agreement with ASTM B962 [13]. This was accompanied by metallographic studies to reveal the microstructural features of the alloy under an optical microscope and SEM. Also, the starting elemental/milled powders and the developed NAB alloys were probed using FESEM). X-ray diffractometer (XRD, Rigaku D/max-rB) was used to identify the phase evolution of the starting, admixed powders, and the sintered alloys to understand the phases formed during the processing and sintering of the alloy. This was carried out by scanning the materials with Cu-Kα ($\lambda = 0.154$ nm) radiation at a rate of 1 °/min over the angular range of 0–90°. Lastly, Vickers microhardness tester (FALCON 500 series) was utilized to measure the microhardness at a load of 100 gf by indenting the polished surfaces of the materials.

3 Results and discussion

3.1 Microstructural analysis of the powders and fabricated NAB alloys

In order to evaluate the microstructural features of the as-received elemental powders, milled powders and the fabricated alloys, the materials were characterized under SEM and the results of the as-received powders are presented in Figure 1a–c. From the SEM images in Figure 1a–c, it was seen that the Cu, Ni and Al powders depict spherical particles.

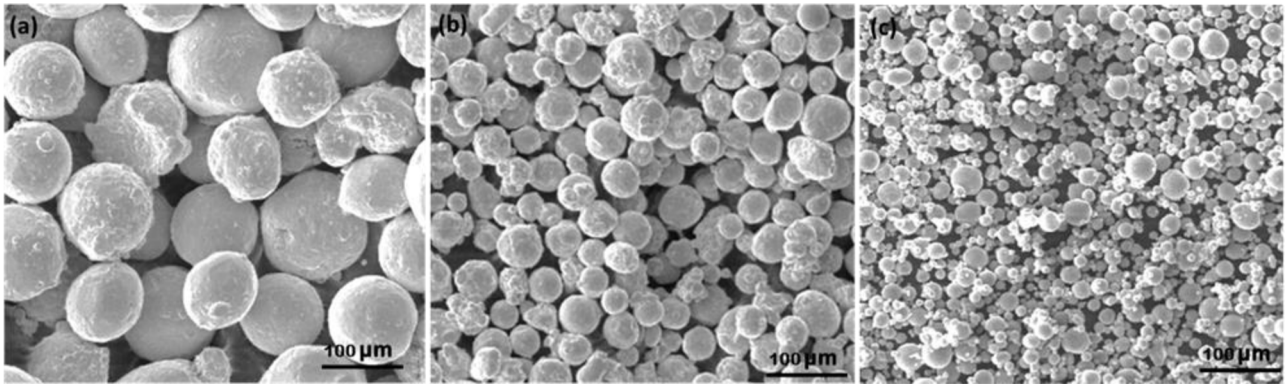

Fig. 1. SEM results of the as-received elemental powders (a) Copper, (b) Nickel and (c) Aluminium.

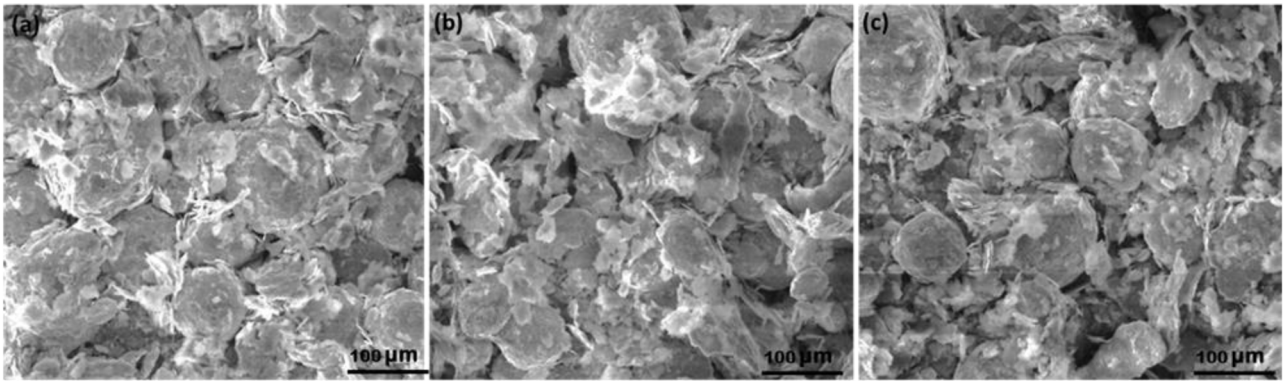

Fig. 2. SEM images of the milled NAB powders which consist of Aluminium (a) 6 wt.%, (b) 8 wt.%, and (c) 10 wt.%.

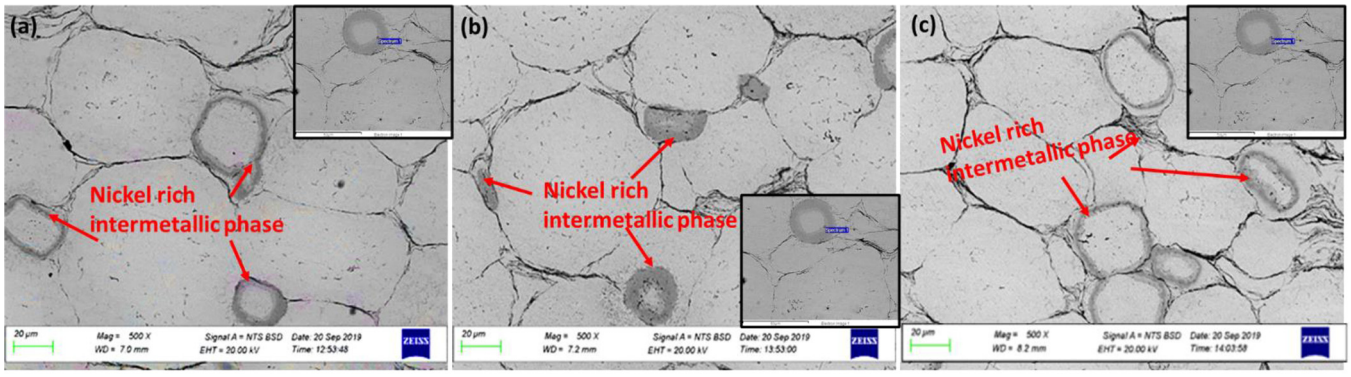

Element	Weight%	Atomic%
Al K	12.11	23.00
Ni K	74.52	65.03
Cu K	13.37	11.97
Totals	100.00	

Fig. 3. SEM micrograph of the sintered NAB alloys which consist of Aluminium (a) 6 wt.%, (b) 8 wt.%, and (c) 10 wt.% alongside the accompanied EDS results to show the composition of the Nickel rich intermetallic phases formed.

On the other hand, the SEM results in Figure 2a–c showed the morphology of the milled powders, which consist of Al of varying concentrations (6, 8 & 10 wt.%). From the results in Figure 2, it was revealed that the powders were homogeneously blended, which confirms the effectiveness of the milling parameters and technique used to mill the starting powders.

Furthermore, it was observed from Figure 2 that the Cu particles were dominant in the powder mixtures, which confirms the concentration of copper in the powders. It was also revealed that the aluminium particles loss their spherical shapes and were uniformly spread across the copper particles after the milling process. The dispersive features of the aluminium in the powder mixture can be attributed to the higher surface area and its malleable nature.

The SEM micrographs of the sintered NAB alloys are shown in Figure 3a–c. From the micrographs which showed the morphology of the fabricated alloys, it was revealed that there was the formation of nickel rich intermetallic phases at the grain boundaries on the alloy which is represented in the EDS result provided. The SEM images showed that the increase in aluminium content up to 10 weight percent resulted in grain refinement within the alloy. The presence of the nickel rich intermetallic phases in the grain boundaries and the refinement of the grains can lead to the improvement of mechanical properties. It has been reported in previous studies that the presence of nickel concentrated region and grain refinements in NAB can result in the improvement of hardness and mechanical strength of the alloy [14,15]. Also, the increase in aluminium content above 8 percent results in the formation of beta phases which is a much stronger and harder phase than the alpha phase that is usually present in NAB at less aluminium content and lower temperature [3]. Additionally, the increase in Al

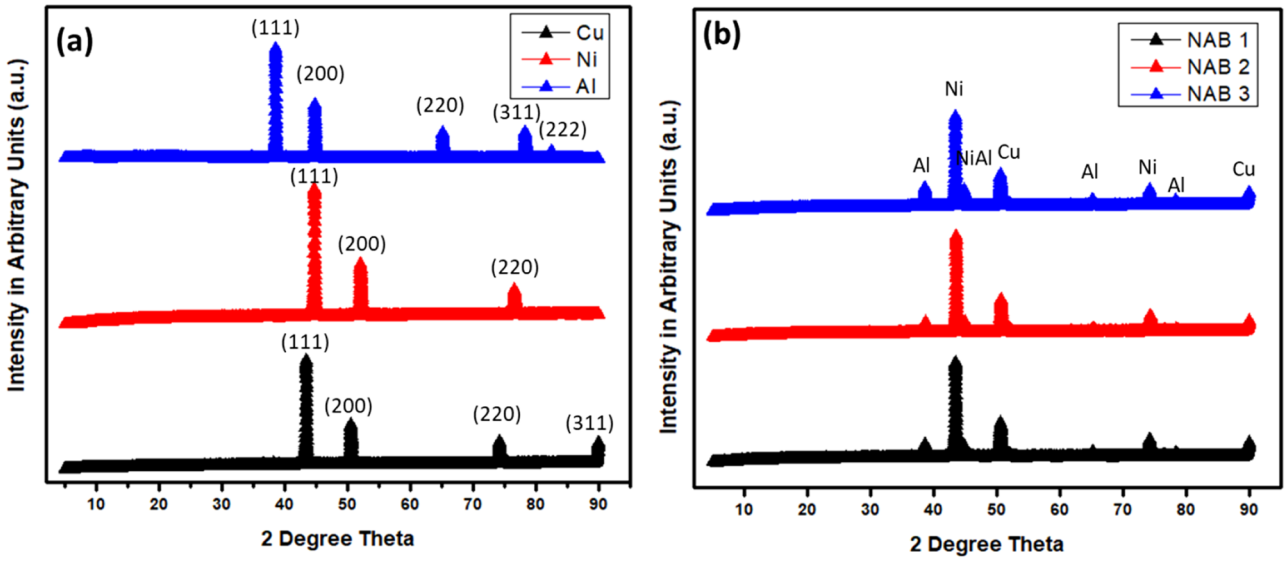

Fig. 4. XRD results of the (a) Starting powders and (b) Mixed powders.

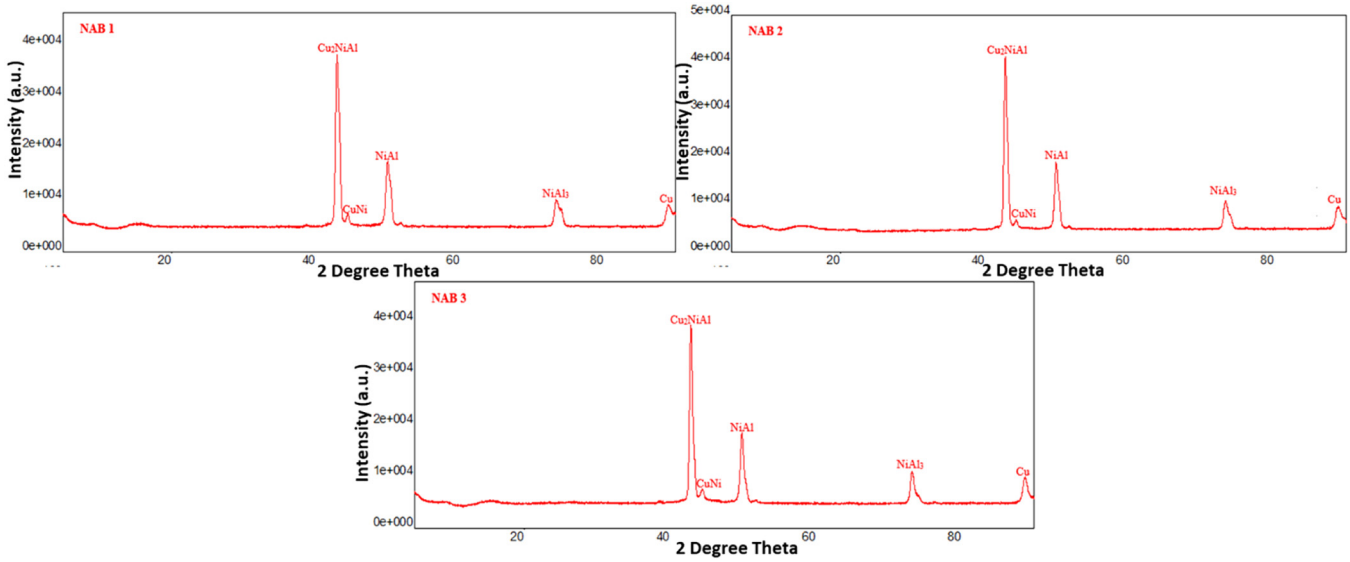

Fig. 5. XRD results of the sintered NAB alloys.

content that results in grain refinement of the NAB alloy can assist in strengthening and improving the corrosion resistance of the alloy [16,17].

3.2 Phase analysis of the powders and the fabricated NAB samples

The phases of the starting elemental powders, milled powders and the fabricated alloys were investigated to reveal the various phases formed as a result of the milling and consolidation process of the NAB alloy and the results are presented in Figures 4a and 4b and 5. The XRD results of the starting elemental powders are shown in Figure 4a and it was revealed from the results of copper that the prominent peaks exist at 2 theta = 43.4°, 50.5°, 74.2° and 91.3° which corresponds to (111), (200), (220) and (311) planes. Similarly, the prominent peaks of nickel powder occurred at 2 theta = 44.7 °, 52.1 ° and 76.6° which coincides with the (111), (200), and (220) planes while the XRD pattern of the aluminium powder depicted the crystallite peaks at 2 theta = 38.5°, 44.8°, 65.2°, 78.3°, and 82.5° which corresponds to (111), (200), (220), (311) and (222) planes. The XRD results of the starting powders showed no traces of other phases, which confirms the high purity of the elemental powders.

Furthermore, the XRD results of the milled powders are presented in Figure 4b and it was revealed that the phases of the elemental powders (Cu, Ni, Al) were prominent. In addition, a new phase (NiAl) was seen in the XRD results of the mixed powders, which implies that a reaction between

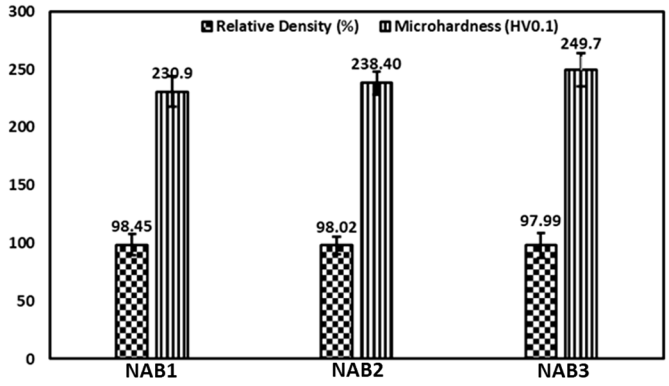

Fig. 6. Relative density and microhardness of the fabricated NAB alloys.

the starting powders occurred during the milling process. Similarly, from the XRD results of the sintered NAB alloys in Figure 5, new intermetallic phases were seen which further corroborate the reaction of the powders during the consolidation process.

3.3 Density and microhardness of the fabricated NAB samples

The density of the fabricated NAB samples which explains the densification of the alloy is shown in Figure 6. From the density results, it was revealed that the increase in aluminium content in the alloy reduced the relative density of the NAB. The relative densities of the sintered alloys were in the range of 97.99–98.45% with the NAB alloy that consists of 6 wt.% (NAB1) showing the best densification value. The decrease in relative density resulting from the increase in aluminium content can be ascribed to the presence of aluminium in the metal structure of the copper particles that restricted the full densification of the sintered alloy [18].

Conversely, the microhardness of the fabricated NAB alloys which is also presented in Figure 6 improved with the increase of aluminium content in the alloy. The improvement in microhardness value of the NAB alloys by the increase in aluminium content can be ascribed to the solid solution and grain refinement and the formation of nickel rich intermetallic phases in the alloy structure. From all indication, the densification of the developed NAB decreases with the aluminium content which is indirectly proportional to the hardness behaviour of the alloy, since the hardness improves with the increase in aluminium content resulting from the grain refinement, the formation of alpha and beta phases and the intermetallic phases in the alloy [19,20].

4 Conclusion

The influence of aluminium content on the microstructure, density and microhardness of SPSed NAB was investigated. From the investigations, it was observed that SPS is a feasible fabrication technique for producing NAB alloys of high relative density. Also, the increase of aluminium content in the fabricated alloys improved the microhardness of the materials. However, the density declined with the increase in aluminium content.

This study was funded by the National Research Foundation of South Africa and the Global Excellence and Stature of the University of Johannesburg South Africa.

References

1. B. Zhang, J. Wang, F. Yan, Load-dependent tribocorrosion behaviour of nickel-aluminium bronze in artificial seawater, Corros. Sci. **131** (2018) 252–263
2. J.A. Wharton, R.C. Barik, G. Kear, R.J.K. Wood, K.R. Stokes, F.C. Walsh, The corrosion of nickel–aluminium bronze in seawater, Corros. Sci. **47** (2005) 3336–3367
3. I. Richardson, Guide to Nickel Aluminium Bronze for Engineers, Copper Development Association Publication No 222, by Copper Alliance, London, United Kingdom (2016), 100
4. A.M. Alfantazi, T.M. Ahmed, D. Tromans, Corrosion behavior of copper alloys in chloride media, Mater. Des. **30** (2009) 2425–2430
5. F. Hasan, A. Jahanafrooz, G.W. Lorimer, N. Ridley, The morphology, crystallography, and chemistry of phases in as-cast nickel-aluminum bronze, Metall. Trans. A **13** (1982) 1337–1345
6. D.R. Ni, P. Xue, Z.Y. Ma, Effect of multiple-pass friction stir processing overlapping on microstructure and mechanical properties of as-cast nial bronze, Metall. Mater. Trans. A **42** (2011) 2125–2135
7. J.R.C. Strang, Nickel-Aluminium Bronze for Seawater: Flattered by Comparison (Shipham Valves, n.d.)
8. W. Zhai, W. Lu, P. Zhang, M. Zhou, X. Liu, L. Zhou, Microstructure, mechanical and tribological properties of nickel-aluminium bronze alloys developed via gas-atomization and spark plasma sintering, Mater. Sci. Eng. A **707** (2017) 325–336
9. Y. Lv, Y. Ding, Y. Han, L.-C. Zhang, L. Wang, W. Lu, Strengthening mechanism of friction stir processed and post heat treated NiAl bronze alloy: effect of rotation rates, Mater. Sci. Eng. A **685** (2017) 439–446
10. A. Dudhmande, T. Schubert, M. Balasubramanian, B. Kieback, Sintering properties of new P/M aluminium alloys and composites, Met Matrix Compos. **1** (2005) 301–306
11. A.M. Okoro, S.S. Lephuthing, S.R. Oke, O.E. Falodun, M.A. Awotunde, P.A. Olubambi, A review of spark plasma sintering of carbon nanotubes reinforced titanium-based nanocomposites: fabrication, densification, and mechanical Properties, JOM (n.d.) **72**, 1–18
12. Z.A. Munir, U. Anselmi-Tamburini, M. Ohyanagi, The effect of electric field and pressure on the synthesis and consolidation of materials: A review of the spark plasma sintering method, J. Mater. Sci. **41** (2006) 763–777
13. A.S. Testing, M.C.B. Metal Powders, M.P. Products, Standard Test Methods for Density of Compacted or Sintered Powder Metallurgy (PM) Products Using Archimedes' Principle (ASTM International, 2009)
14. S. Nair, R. Sellamuthu, R. Saravanan, Effect of nickel content on hardness and wear rate of surface modified cast aluminum bronze alloy, Mater. Today Proc. **5** (2018) 6617–6625

15. B. Zhao, Y. Lv, Y. Ding, L. Wang, W. Lu, Materials characterization the grain re fi nement mechanisms of various phases in shot-peened Nickel- Aluminum bronze (NAB) alloy, Mater. Charact. **144** (2018) 77–85
16. Z. Qin, Z. Wu, X. Zen, Q. Luo, L. Liu, W. Lu et al., Improving corrosion resistance of a nickel-aluminum bronze alloy via nickel ion implantation, Corrosion **72** (2016) 1269–1280
17. U. Donatus, J.A. Omotoyinbo, I.M. Momoh, Mechanical properties and microstructures of locally produced aluminium-bronze alloy, J. Miner. Mater. Charact. Eng. **11** (2012) 1020–1026
18. A.M. Okoro, R. Machaka, S.S. Lephuthing, S.R. Oke, M.A. Awotunde, P.A. Olubambi, Evaluation of the sinterability, densification behaviour and microhardness of spark plasma sintered multiwall carbon nanotubes reinforced Ti6Al4V nanocomposites, Ceram. Int. **45** (2019)
19. M. Kaplan, A.K. Yildiz, The effects of production methods on the microstructures and mechanical properties of an aluminum bronze, Mater. Lett. **57** (2003) 4402–4411
20. S. Öztürk, S.E. Sünbül, A. Metoglu, K. İÇİN, Improvement of microstructure, tribology and corrosion characteristics of nickel-aluminum bronze by P/M method, Tribol. Int. **151** (2020) 106519

Cite this article as: Avwerosuoghene Moses Okoro, Senzeni Sipho Lephuthing, Samuel Ranti Oke, Peter Apata Olubambi, Influence of aluminium content on the microstructure and densification of spark plasma sintered nickel aluminium bronze, Manufacturing Rev. **8**, 9 (2021)